Transition crossing in proton synchrotrons using a flattened rf wave

C. M. Bhat, J. Griffin, J. MacLachlan, M. Martens, K. Meisner, and K. Y. Ng
Fermi National Accelerator Laboratory, P.O. Box 500, Batavia, Illinois 60510
(Received 12 December 1995; revised manuscript received 4 October 1996)

The problems of beam loss and emittance growth during transition crossing in a proton synchrotron have been major issues for many years. Recently we have developed a scheme that resolves some of these problems by eliminating rf focusing during transition crossing. The technique uses a flattened (nonsinusoidal) rf wave form which delivers the correct acceleration to all particles in the beam. This scheme has been tested in the Fermilab Main Ring accelerator by the addition of 13% of a third harmonic rf voltage to the fundamental accelerating rf voltage during the nonadiabatic period near the transition energy. Beam loss was completely eliminated, and longitudinal emittance dilution after transition remained below 15%. Simulations of longitudinal beam dynamics reproduce the data well. [S1063-651X(97)10001-0]

PACS number(s): 29.27.Bd, 29.27.Fh, 41.75.Ak

I. INTRODUCTION

A. Overview

Half a century ago, Veksler [1] and McMillan [2] demonstrated how ensembles of charged particles (*bunches*) with a small momentum spread around some *synchronous momentum* p_s may be accelerated at nearly constant orbit radius, in an increasing magnetic guide field. The accelerating fields are generated by radio frequency (rf) resonant cavities operating at a frequency $\omega_{rf}/(2\pi)$ equal to an integer h (*harmonic number*) times the revolution frequency $\omega_s/(2\pi)$ of the synchronous particle. An off-momentum particle with a fractional momentum deviation $\delta=\Delta p/p_s$ follows a different closed orbit from that of the synchronous particles. The deviation of the revolution period from the synchronous period T_s is characterized by the *phase slip factor* η_0, defined by [3]

$$\frac{\Delta T}{T_s}=\left[\alpha_0-\frac{1}{\gamma_s^2}\right]\delta=\eta_0\delta, \tag{1.1}$$

where the lattice parameter α_0 (*momentum compaction factor*) measures the fractional change in orbit length $\Delta C/C_s$ for each unit fractional deviation in particle momentum δ, i.e.,

$$\frac{\Delta C}{C_s}=\alpha_0\delta. \tag{1.2}$$

In Eq. (1.1) γ_s is the ratio of the energy of the synchronous particle E_s to its rest energy E_0. During the acceleration of the beam particles, when $\gamma_s=\gamma_T=\alpha_0^{-1/2}$, the phase-slip factor changes sign. This instant of acceleration is called *transition crossing* and the corresponding energy $\gamma_T E_0$ is the transition energy.

The synchronous particles are accelerated as they traverse the rf cavity gaps at a *synchronous phase angle* ϕ_s by an effective accelerating voltage $V_{acc}=V_{rf}\sin\phi_s$. Here the V_{rf} is the peak voltage of the sinusoidal rf wave. A particle with energy offset ΔE arrives at the rf cavity at a different time and therefore sees a different rf phase angle $\phi=\phi_s+\Delta\phi$. The slip in $\Delta\phi$ is governed by

$$\frac{d\Delta\phi}{dt}=\frac{h\eta_0\omega_s}{\beta_s^2E_s}\Delta E, \tag{1.3}$$

where β_s is the ratio of the velocity of the synchronous particle to the velocity of light. Hence an off-energy particle receives additional energy from the rf cavities at the rate of

$$\frac{d\Delta E}{dt}=\frac{eV_{\rm rf}\omega_s}{2\pi}[\sin(\phi_s+\Delta\phi)-\sin\phi_s]. \tag{1.4}$$

Equations (1.3) and (1.4) form the equations of motion of a particle in the longitudinal phase space $(\Delta E,\Delta\phi)$. For small $\Delta\phi$ and ΔE, particles perform *synchrotron phase oscillations* with frequency

$$f_{\rm syn}=\left(-\frac{eh\eta_0V_{\rm rf}\cos\phi_s}{2\pi\beta_s^2E_s}\right)^{1/2}\frac{\omega_s}{2\pi}, \tag{1.5}$$

provided $\eta_0\cos\phi_s<0$. To maintain phase stability during acceleration across the transition energy, the synchronous phase must switch from $0<\phi_s<\frac{1}{2}\pi$ to $\frac{1}{2}\pi<\phi_s<\pi$. When $V_{\rm rf}>2\pi(dp_s/dt)\beta_sc/e\omega_s$ and $0<\sin\phi_s<1$ then there is a range of ϕ and δ for which the particles have stable synchrotron oscillations. The stable region which determines the maximum possible extent of a bunch is referred to as an rf *bucket*. The phase-space area occupied by a bunch of particles is referred to as *longitudinal emittance*.

B. Problems encountered in transition crossing

During acceleration the off-momentum particles can be accorded the same average acceleration as synchronous particles because of the synchrotron phase oscillation. But stable oscillatory motion of the particles inside the bucket exists only when the parameters in the equations of motion change adiabatically. The height of the bucket, however, has the property,

$$(\Delta E)_{\text{bucket}} \propto \left(\frac{E_s}{|\eta_0|} \right)^{1/2} \tag{1.6}$$

with rapidly changing η_0^{-1} around transition. Then, from Eq. (1.2) and assuming that the rate of change of γ_s is constant near transition, we obtain,

$$\eta_0 = \frac{2\dot{\gamma}_s t}{\gamma_s^3}. \tag{1.7}$$

The time t is measured from the moment when the synchronous particle crosses the transition. Thus, as transition is approached, synchrotron frequency is reduced to zero while the bucket height is increased to infinity according to Eqs. (1.5) and (1.6). Therefore the particles unable to catch up with the rapid changes in the bucket shape. This time interval $-T_{\text{na}}$ to $+T_{\text{na}}$ is the *nonadiabatic period*, and T_{na} is the *nonadiabatic time*. Quantitatively, this period is defined by

$$f_{\text{syn}} \leqslant \frac{2}{(\Delta E)_{\text{bucket}}} \frac{d(\Delta E)_{\text{bucket}}}{dt}, \tag{1.8}$$

from which one gets [3]

$$T_{na} = \left[\left(\frac{\beta_T^2 \gamma_T^4}{2\omega_s h} \right) \left(\frac{|\tan\phi_s|}{\dot{\gamma}_T^2} \right) \right]^{1/3}, \tag{1.9}$$

where the subscript T implies evaluation of corresponding quantities at transition.

During the nonadiabatic time, the phase of the particles in an rf bucket is almost frozen, as per Eq. (1.3), i.e., the leading and the lagging particles in a bunch remain in their relative positions; thus they continue to gain or lose energy from the rf cavities [see Eq. (1.4)]. As a result, the momentum spread increases rapidly, and may exceed the momentum aperture of the accelerator leading to beam loss.

Another characteristic feature of transition crossing arises from the fact that different beam particles in a bunch cross transition at different times. Because of the energy dependence of the momentum-compaction factor, each particle has a different γ_T depending on the deviation of its energy from the synchronous energy. When this energy dependence is taken into account, Eq. (1.2) is replaced by [4],

$$\frac{\Delta C}{C_s} = \alpha_0 \delta [1 + \alpha_1 \delta + O(\delta^2)]. \tag{1.10}$$

For a particle with momentum offset δ, $\gamma_T(\delta)$ becomes

$$\gamma_T^{-2}(\delta) = \frac{dC/C}{dp/p} = \alpha_0 [1 + (2\alpha_1 + 1 - \alpha_0)\delta + O(\delta^2)]. \tag{1.11}$$

A particle with peak momentum spread $\hat{\delta}$ crosses transition earlier than the synchronous particle, by a time [4,5]

$$T_{\text{nl}} = \frac{\gamma_T \hat{\delta}}{\dot{\gamma}_s} \left(\alpha_1 + \frac{1 + 2\beta_s^2}{2} - \frac{\alpha_0}{2} \right). \tag{1.12}$$

This time is called the *nonlinear time*. There is a period during which some particles are above transition while others are below. If the rf transition phase jump is set at the time when the synchronous particle crosses transition, the particles with higher momentum spend a substantial period above transition prior to the rf phase jump. Such particles are effectively outside of the bucket. They are subject to a defocusing force and move along hyperbolic divergent paths, thus producing a tail in the longitudinal phase space distribution. In contrast to this, particles with momentum lower than the synchronous momentum experience a defocusing force as soon as the rf phase is switched, and they also move along divergent paths producing a second tail in the phase-space distribution. The consequence of the growth of two tails in $(\Delta E, \Delta\phi)$ phase space is the shape mismatch between the distribution and the bucket following the transition which in turn leads to longitudinal emittance dilution. If the tails extend beyond the bucket or the momentum aperture of the accelerator, there is beam loss.

The other problems during transition crossing include, the interaction of the beam with the coupling impedance of the vacuum chamber, and, a vanishing η that implies the loss of Landau damping, leading to the microwave and the negative mass instabilities [6,7].

Several techniques have been suggested [8] to cure the problems of beam loss and longitudinal emittance dilution during transition crossing. One method that has been successfully employed in slow-ramping synchrotrons is the γ_T -jump scheme [6,9–11]. Implementation of a γ_T −jump scheme in a fast-ramping synchrotron is quite challenging and expensive.

Recently we have developed a scheme [12–14] which employs rf manipulation using a flattened (nonsinusoidal) rf wave in the vicinity of transition. With this technique, all particles are accelerated equally during the nonadiabatic and nonlinear periods so that excessive growth in momentum offset does not occur. Thereby the beam emittance growth can be minimized and beam loss arising from nonlinear and nonadiabatic effects can be eliminated. The principle of the technique is described in detail in Sec. II. The results from an experimental test of the technique in the Fermilab Main Ring are presented in Sec. III.

II. CONCEPTS OF TRANSITION CROSSING USING A FLATTENED RF WAVE

The growth of momentum spread near transition is the consequence of the loss of adiabaticity in the presence of normal rf focusing. The basic idea of the transition crossing using a flattened rf wave is the creation of an rf accelerating wave which is constant in amplitude over the fundamental rf phase range occupied by particles in each bunch. This rf wave is to provide for all particles exactly the same accelerating voltage required to hold synchronous particles near the center of the vacuum chamber aperture, i.e., $V_{\text{acc}} = 2\pi(dp_s/dt)\beta_s c/e\omega_s$. The flattened rf condition is maintained during a time interval of $-\Delta T$ to $+\Delta T$, where one may choose $\Delta T = (T_{\text{na}} + T_{\text{nl}})$. The normal sinusoidal rf wave is replaced by the flattened rf wave at time $-\Delta T$. This removes the rf phase focusing during the transition crossing period. The choice of $\Delta T = (T_{\text{na}} + T_{\text{nl}})$ is appropriate because

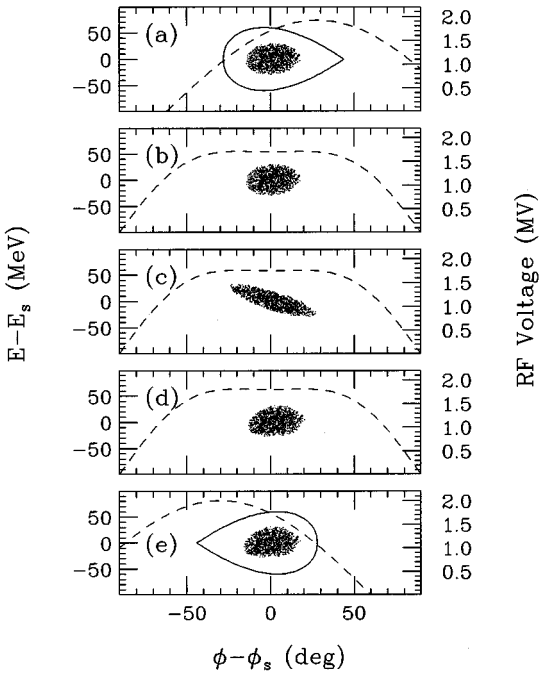

FIG. 1. Evolution of particle distribution in a bunch from beginning to the end, simulated using ESME [15] for transition crossing with flattened rf wave. No buckets sepatracies are shown in (b), (c), and (d) because longitudinal focusing has been eliminated during nonadiabatic and nonlinear period near transition. The rf wave forms with appropriate amplitudes are shown by dashed curves.

the particles with the maximum (minimum) momentum spread cross transition at $\mp T_{\rm nl}$, and, the nonadiabatic time period $\pm T_{\rm na}$ is measured from their respective times of transition crossing. In essence, the nonsinusoidal rf transition crossing described here, eliminates the rf focusing during the transition crossing interval from $-\Delta T$ to $+\Delta T$, which in turn prevents the unwanted increase in the momentum spread, while providing the correct accelerating voltage to all particles in a bunch.

We show in Fig. 1 the evolution of phase-space distribution of particles in a bunch as they are accelerated through transition energy with flattened rf wave. This illustration comes from the results of a multiparticle longitudinal beam dynamics simulation using a computer code called ESME [15]. (These simulations are discussed later in this section). Figure 1(a) shows the distribution of particles below transition inside a moving bucket. At time $-\Delta T$, the nonsinusoidal rf is applied [see Fig. 1(b)]. Particles with positive momentum deviation δ shear slowly to earlier time with the converse being true for those with negative δ, as depicted in Fig. 1(c). As particles cross γ_T, they reverse their direction of relative motion and shear toward the center of the distribution as shown in Fig. 1(d). At the end of the transition crossing, i.e., at $+\Delta T$, when all particles are above transition, the original sinusoidal rf condition is resurrected with the synchronous phase switched to the negative slope of the sinusoidal rf wave [see Fig. 1(e)]. The net effect of the entire process on the line charge current (the projection of the charge distribution on the phase axis) is that the bunch becomes longer with decreased peak current as transition is approached, then narrows toward its original length by the end of time ΔT. Because particles with lower momentum remain below transition for a longer period the final distribution is slightly distorted and its centroid displaced slightly toward later time [12]. However, except for instability growth, space-charge effects and higher-order lattice effects, the final momentum spread of the distribution should remain unchanged.

If the coupling impedance seen by the the bunch is predominantly inductive (capacitive—if, only the space-charge force is taken into account), then the bunch has a tendency to decrease (increase) in length below transition and increase (decrease) in length above transition [8,16]. In the transition crossing process described here, as each part of the distribution passes through transition, the additional decrease (or increase) in bunch length below transition is approximately compensated by the opposite change that takes place above the transition. Therefore, this effect of the impedance on the bunch is minimized. However, complications arise due to nonlinear effects, microwave and negative mass instabilities which alter the situation.

As is evident from Fig. 1, the constant voltage portion of the rf wave must extend over sufficient time or phase to encompass the maximum extent of distribution shearing which occurs during ΔT. From Eq. (1.3), particles at the extreme momentum spreads $\pm\hat{\delta}$ in the distribution shear to a maximum phase extent of

$$\Delta\phi|_{\rm max}=\int_{-\Delta T}^{0}\ \text{or}\ \int_{0}^{\Delta T}h\omega_s\eta\hat{\delta}dt. \tag{2.1}$$

To compute this integral we need higher orders of the phase-slip factor, i.e., Eq. (1.1) should be written as ,

$$\frac{\Delta T}{T_s}=[\,\eta_0+\eta_1\delta+O(\delta^2)\,]\delta. \tag{2.2}$$

Using Eqs. (1.7) and (1.10) we get,

$$\eta\approx\frac{2\dot{\gamma}_s t}{\gamma_s^3}+\left(\alpha_0\alpha_1+\frac{3\beta_s^2}{2\gamma_s^2}\right)\delta. \tag{2.3}$$

Thus the particles at the extreme momenta $\pm\hat{\delta}$ in the distribution can have maximum phase extent,

$$\Delta\phi|_{\rm max}=\frac{h\omega_s\hat{\delta}\Delta T}{\gamma_T^2}\left[\frac{\dot{\gamma}_T\Delta T}{\gamma_T}+\left(\alpha_1+\frac{3\beta_s^2}{2}\right)\hat{\delta}\right]. \tag{2.4}$$

Since the initial longitudinal emittance must have a finite phase extent as well as momentum spread, the maximum extent of the sheared distribution will be slightly larger than the extent given above. The actual extent depends on the initial longitudinal emittance, on the aspect ratio (ΔT versus ΔE), and on the sign and magnitude of α_1. Equation (2.4) also represents the minimum required extent of the rf phase where the amplitude of the rf wave is held constant.

The transition crossing with flattened rf wave described above has been studied under different conditions of bunch intensities and longitudinal emittances using the simulation code ESME [15]. The code allows one to vary the chromatic

TABLE I. Dynamic parameters of the Fermilab Main Ring.

Radius of ring	1.0 km
Rf harmonic h	1113
Transition gamma γ_T	18.85
Transition momentum p_t	17.665GeV/c
Ramp rate at transition $\dot{\gamma}_T$	89.17 s^{-1}
First-order momentum compaction α_1	0.83 ($0.81 \pm 30\%$ [a])
Fundamental rf voltage	2.2 MV (max) at 53 MHz
3rd harmonic rf voltage	280 kV (max) at 159 MHz
Initial emittance	0.05 to 0.2 eV-s
Bunch intensity	up to 2.5×10^{10} ppb
Momentum aperture at transition $\hat{\delta}$	0.003 [b]
Impedance $Z_\parallel/n$	3.0 Ω ($1.4\Omega \leqslant Z_\parallel \leqslant 8.6\Omega$ [c]
Average beam pipe radius	0.025 m
Cutoff frequency	3.42 GHz

[a]Reference [17].
[b]Reference [18], equivalent to 0.01 m.
[c]References [19] and [20].

factor α_1, space charge, and vacuum chamber impedance effects (including those of lumped resonators), and particle distribution. All tracking calculations were made with 10^6 macroparticles and 13.5 GHz cutoff of the beam current spectrum. Figure 1 used as an illustration before is an example of such a calculation performed using the dynamic parameters of the Fermilab Main Ring listed in Table I. In this calculation the beam intensity was 2.5×10^{10} protons per bunch with longitudinal emittance of 0.09 eV s. The increase in momentum spread over the period $2\Delta T$ appears to be negligible although an increase in the longitudinal emittance of approximately 15% is evident. The final distribution is reasonably well matched to the reapplied contour of the focusing bucket. The initial line charge projection was parabolic with full bunch length of the order of 1.7 ns. Space-charge and ring impedance effects were also included in the calculation. The duration of the flattened rf wave condition was ± 6.5 ms. With a momentum spread of $\pm 2\times10^{-3}$ from Fig. 1(a), Eq. (2.4) gives a maximum phase spread of $\Delta\phi|_{\max} \approx 50°$ for the highest momentum particles. The full shear as can be seen in Fig. 1(c) is about 53°. This gives an indication of the extent of the constant voltage phase range required for the procedure.

The most difficult aspect of transition crossing with flattened rf wave is the proper selection of the phase and amplitude at the end of the process so as to best match the bucket shape to the final distribution. An improper match results in quadrupole oscillations of the mismatched bunch within the bucket (tumbling) and filamentation due to the spread in synchrotron tune. The apparent longitudinal emittance of the bunch eventually fills the contour within which the tumbling occurs. The first and foremost source of the problem is the difference in shape between the accelerating focusing buckets before $t=-\Delta T$ and after $t=\Delta T$ [see Figs. 1(a) and 1(e)]. The second cause is the nonlinearity of the shearing as per Eq. (1.3), due to the η_1 term in Eq. (2.2). In the presence of an accelerating but nonfocusing rf field the particles in a bunch with $\delta>0$ and $\delta<0$ shear according to

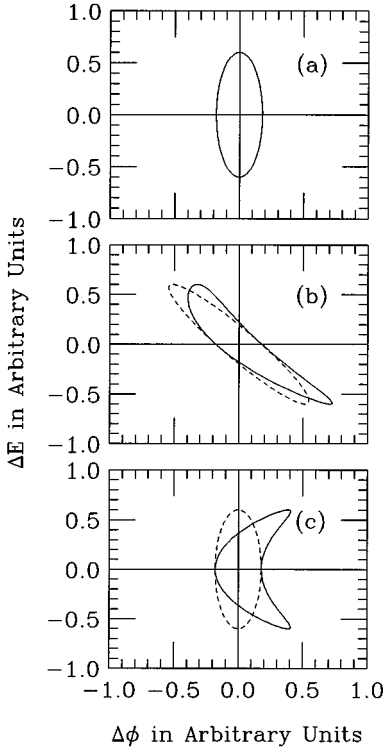

FIG. 2. Phase-space distribution of particles in a bunch with a constant amplitude rf wave calculated using Eq. (2.5): (a) the energy of particles in the bunch are below transition energy E_T, (b) the energy of the synchronous particles are at E_T, and (c) the energy of particles in the bunch are above E_T. The solid and dashed curves are calculated with and without higher-ordered terms included in the expansion of the slip factor η.

$$-\Delta T<t<0\rightarrow\begin{cases}-|\eta_0|\delta+\eta_1\delta^2 & \delta>0\\ |\eta_0||\delta|+\eta_1\delta^2 & \delta<0\end{cases}$$

$$0<t<\Delta T\rightarrow\begin{cases}\eta_0\delta+\eta_1\delta^2 & \delta>0\\ -\eta_0|\delta|+\eta_1\delta^2 & \delta<0\end{cases}. \quad (2.5)$$

The shearing of the particle distribution calculated from Eq. (2.5) with $\eta_1\neq0$ and $\eta_1=0$ are shown in Fig. 2 by solid and dashed curves, respectively. When $\eta_1\neq0$, particles with $\delta>0$ shear less to the left but shear back more to the right, while particles with $\delta<0$ shear more to the right but shear back less to the left. The bunch shape at $t=\Delta T$ is therefore differ from that at $t=-\Delta T$. Thus, instead of being an approximate parabolic bunch, the distribution has the appearance of an Australian boomerang [see Fig. 2(c)] with the vertex facing left, indicating the sensitivity of the shape of the final distribution to η_1. In this context, particle tracking simulations have shown that better matches can be achieved by adjusting the start and stop times of the perturbed rf wave in an asymmetrical manner about the transition time.

The required flattop rf wave can be generated by superposing a second or third harmonic of proper phase and amplitude on the fundamental rf wave. For example, an addition of 28% second harmonic or 13% third harmonic to the fundamental sine wave produces a combined wave form which is constant in voltage to within $\pm 0.3\%$ over 76° or 54°, respectively. In actual implementation, several feedback

loops must be operational. The amplitude and relative phase of the fundamental and the chosen harmonic must be measured independently and their ratio carefully controlled. The phase of the combined wave must be controlled by comparison with the phase of the centroid of the beam bunches in the machine. Finally, the amplitude of the combined wave must be dynamically controlled by feedback from measurement of the mean beam radial position. Each of these feedback systems is slightly different from those normally used in acceleration, so a carefully designed switching system must be implemented to make the system operational during the interval $-\Delta T$ to ΔT.

It is worth mentioning that use of second or third harmonic wave additions to the rf voltages of isochronous cyclotrons have been reported [21,22] previously. The rf manipulation described here for the crossing transition in a high energy synchrotron is, however, first of its kind.

III. EXPERIMENTAL STUDIES AND RESULTS

The experiment was conducted in the Fermilab Main Ring by implementing a flattened rf wave during transition crossing. The Main Ring is a 150 GeV proton synchrotron with $\gamma_T = 18.85$. Bunches with intensity up to 2.3×10^{10} protons per bunch and longitudinal emittance in the range 0.07 to 0.10 eV s are injected from a Booster synchrotron at 8.938 GeV. ($\gamma_{\text{Injection}} = 9.526$). The fundamental rf system, at $h=1113$, consists of sixteen rf cavities capable of generating rf accelerating voltage between 1 and 4.2 MV in the frequency range 52.813 to 53.104 MHz.

From injection until just above transition energy the momentum of the particle in the Main Ring increases approximately parabolically,

$$p_s(t)=(8.889+200t^2)\text{GeV}/c. \tag{3.1}$$

Here t is the time measured from the beginning of the acceleration cycle. In the Main Ring, the transition crossing is routinely accomplished by lowering the rf voltage toward that required for acceleration at γ_T, switching the sinusoidal rf phase from positive slope to negative slope and by rapidly raising the voltage to establish the post-transition bucket. This procedure results in 5-6% beam loss and an emittance dilution up to about a factor of 2.5 at transition. A previous study of transition crossing in the Main Ring [23] has demonstrated that the beam loss is correlated to the initial longitudinal emittance and increases with it. The observed beam loss is apparently related to the growth in momentum spread beyond the ring momentum aperture of $\approx 0.3\%$ [18]. Hence the Main Ring is a suitable synchrotron to test the new scheme.

The total nonadiabatic and nonlinear time, $-\Delta T$, for the Main Ring is about 5 ms. During the transition crossing interval from -5 ms to 5 ms the fundamental rf frequency changes by about 7.2 kHz. A suitable third harmonic rf system would be required to deliver in excess of 270 kV at 159 MHz, tunable over a range of 22 kHz. An rf system capable of meeting these requirements was developed [24–27] using a prototype CERN cavity [28,29] and was installed in the Main Ring.

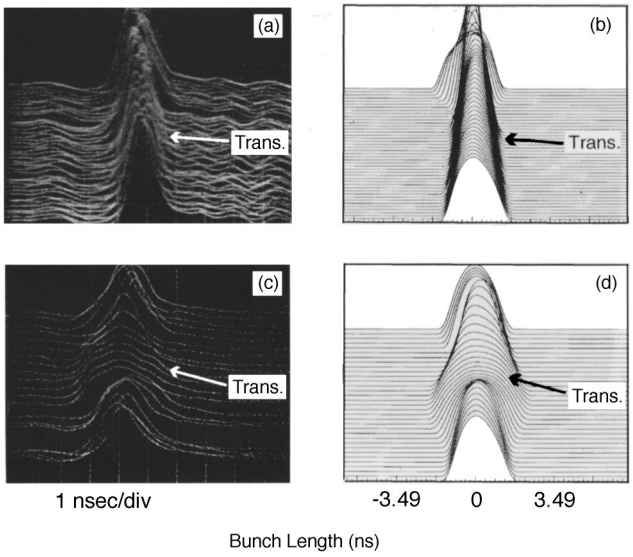

FIG. 3. Mountain-range (evolution of particle distribution in a bunch as a function of time) plots for normal [(a) and (b)] and transition crossing with flattened rf wave [(c) and (d)] in the Main Ring. The total time span along y axis in these figures is about 19 ms. Approximate position of the transition is also shown in each figure. The mountain range data shown in (a) and (c) are obtained from a resistive wall pickup detector in the Main Ring. (b) and (d) are predicted mountain range from ESME simulations. The duration of transition crossing with flattened rf wave was about 12 ms.

The transition crossing studies with flattened rf wave were conducted under beam conditions similar to the normal operation of the accelerator. On each accelerating cycle, a train of 13 bunches with intensity ranging from 0.3 to 2.3×10^{10} protons per bunch was accelerated through transition. The initial longitudinal emittance of the bunches was varied over the range 0.07 to 0.10 eV s. Longitudinal emittances were inferred by the measurements of bunch length [30], V_{rf}, ϕ_s, and p_s at times 20 ms before and after the transition. The error in the longitudinal emittance is estimated to be about 15%.

Typical mountain-range plots showing the time evolution of bunch shape during transition crossing for normal and flattened rf wave conditions are displayed in Figs. 3(a) and 3(c). The predicted bunch lengthening near transition is clearly observed. Figures 3(b) and 3(d) are the results of simulations carried out using ESME under the same beam conditions.

Figure 4(a) is a portion of a typical ''snap shot'' of data obtained at the accelerator console during the normal acceleration scheme. The beam intensity was 1.74×10^{10} protons per bunch with initial longitudinal emittance of 0.07 eV s. The top trace is the beam current, which shows $\sim 5\%$ drop just following transition. The lower trace is the bunch length. As expected the bunch length reached a minimum value near transition. Following transition the trace shows large oscillations in bunch length at twice the synchrotron frequency, indicative of tumbling within the bucket resulting from the large momentum ''tails'' extending to the bucket boundaries. Figure 4(b) shows a similar plot for the transition crossing with flattened rf wave. The initial beam conditions are similar to one shown on Fig. 4(b). No beam loss occurred. The

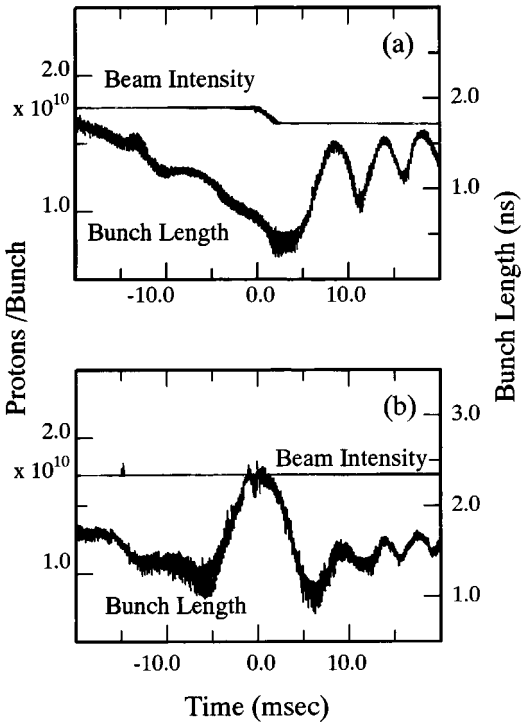

FIG. 4. Typical ''snap-shot'' plots of the beam intensity and the bunch length during a 40 ms period centered on the transition time for (a) normal transition crossing and (b) with flattened rf wave. Other traces normally showing beam radial position and rf phase have been removed for clarity. Initial longitudinal emittances in both these cases were 0.07 ± 0.01 eV s.

bunch length passed through a maximum ~ 2.4 ns (46° of the fundamental rf period) near transition as expected, and length oscillations were small following transition. Figure 5 shows ESME simulations of the data shown in Fig. 4. The agreement between experimental data and their predictions is good. The beam loss at transition for the normal transition crossing is coming from the limited momentum aperture. In the case of transition crossing with flattened rf wave, the beam intensity (not shown in Fig. 5) remained unchanged at 1.73×10^{10} particles per bunch throughout the transition crossing.

Transition crossing data with flattened rf wave were taken up to the maximum available beam intensity of 2.3×10^{10} protons per bunch with longitudinal emittance up to 0.11 eV s. Under these conditions no beam loss was observed and the longitudinal emittance growth was limited to $\approx 15\%$.

All these data with the new scheme were taken setting the $\Delta T = 6$ ms, symmetrically on the both side of transition time. Because the particles in the bunch do not shear linearly with momentum the time symmetry does not amount to momentum symmetry about the transition. If $\hat{\delta}$ is large, then one expects the maximum bunch length to exceed the extent of flattened rf voltage range. In order to compensate for this possibility, data were taken over a range of ''on'' and ''off'' times. Studies with the maximum available beam intensity and with different longitudinal emittance did not indicate that there was any advantage to be gained by introducing asymmetry in crossing the transition with flattened rf wave. Also it was found that reduction of the symmetric crossing time by up to about 30% did not alter the results.

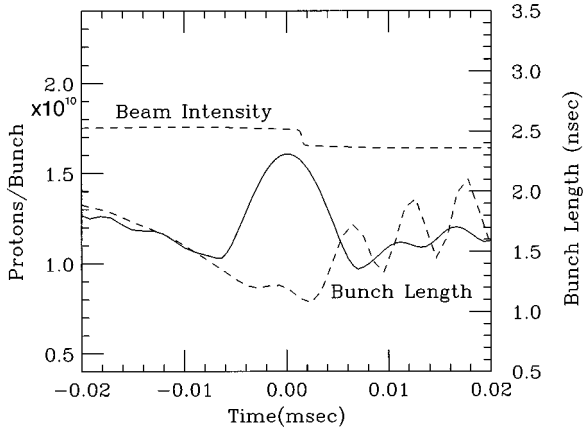

FIG. 5. Multiparticle ESME simulations corresponding to the data shown in Figs. 4(a) and 4(b). The solid and dashed curves show simulations for the transition crossing with flattened rf wave and normal transition crossing schemes, respectively. In the case of transition crossing with flattened rf wave, the duration of the transition crossing time was 12 ms and the simulation was carried out with a beam intensity of 1.73×10^{10} particles per bunch which remained unchanged; for clarity the beam intensity is not shown.

IV. CONCLUSIONS

The beam loss and longitudinal emittance growth during acceleration across the transition energy in a synchrotron have been a major problem for many years. Recently we have developed a scheme which involves the introduction of a flattened rf wave form, where rf focusing is removed for a period of time and all particles in each bunch are accorded just the required accelerating voltage per turn during the nonadiabatic and nonlinear periods near transition. A method to determine the amount of bunch shearing and the required extent of the rf phase where the rf amplitude is held constant during transition crossing is presented.

A third harmonic rf system in combination with the fundamental rf system, which produce constant rf voltage in the phase range of $\approx 54°$ was developed to test the scheme in the Fermilab Main Ring accelerator. It has been demonstrated that beam loss at transition can be completely eliminated up to the maximum available beam intensity of 2.3×10^{10} protons per bunch. With incident longitudinal emittance up to 0.10 eV s per bunch, the emittance growth was limited at transition to less than 15%.

ACKNOWLEDGMENTS

The authors would like to thank D. Wildman for his help during the experiment, and S. D. Holmes, S. Y. Lee, and P. S. Martin for useful discussions and comments. Thanks are also due to C. Crawford, J. Dey, I. Kourbanis, and S. Peggs for help during the work. The authors would also like to acknowledge the help and co-operation from Fermilab Accelerator Operation, Control, and Instrumentation groups. The Fermi National Accelerator Laboratory is operated by The Universities Research Association under contract with the U. S. Department of Energy.

[1] V. Veksler, J. Phys. U.S.S.R. **9,**153 (1945).
[2] E. McMillan, Phys. Rev. **68,** 143 (1945).
[3] E. D. Courant and H. S. Snyder, Ann. Phys. (N.Y.) **3,** 1 (1958).
[4] K. Johnsen, Proc. CERN Symp. High Energy Accelerators Pion Phys. **1**, 106 (1956).
[5] S. Y. Lee and J. Wei, *Non-linear Synchrotron Motion Near Transition Energy in RHIC*, Proceedings of the European Particle Accelerator Conf., Rome, Italy, June 7–11, 1988, edited by S. Tazzari (World Scientific, Singapore, 1989), Vol. 1, pp. 764–766.
[6] W. Hardt *et al.*, Proceedings of the 8th International Conference on High Energy Accelerators, Geneva, 1971, p. 323.
[7] S. Y. Lee and J. M. Wang, IEEE Trans. Nucl. Sci. **32** (5), 2323 (1985).
[8] A. Sorenssen, Part. Accelerators **6,** 141 (1975).
[9] W. Hardt, *Proceedings of the IXth International Conference on High Energy Accelerators* (SLAC, Stanford, CA, 1974), pp. 434–438.
[10] W. K. van Asselt *et al.*, *IEEE Proceedings of the 1995 Particle Accelerator Conference and International Conference on High Energy Accelerators, Dallas* (IEEE, New York, 1996), p. 3022.
[11] W. Merz *et al., Proceedings of the IEEE Particle Accelerators Conference March 16-19, 1987, Washington, D.C.*, edited by E. R. Lindstorm and L. S. Taylor (IEEE, New York, 1987), p. 1343.
[12] J. Griffin, Fermilab Report No. TM-1734, 1991 (unpublished).
[13] J. Griffin and C. M. Bhat, Fermilab Report No. MI-0062, 1991 (unpublished).
[14] J. A. MacLachlan *et al.*, Int. J. Mod. Phys. A (Proc.Suppl.) **2B,** 1040 (1993).
[15] J. A. MacLachlan, Fermilab Report No. FN-529, 1989 (unpublished); J. A. MacLachlan, Fermilab Report No. FN-481, 1988 (unpublished).
[16] A. Hofmann, in *Theoretical Aspects of the Behaviour of Beams in Accelerators and Storate Rings*, Proceedings of the First Course of the International School of Particel Accelerators of the ''Ettore Majorana'' Center for Scientific Culture Erice 10-22, 1976 (CERN, Geneva, 1977), CERN Report No. 77-13, p. 139.
[17] K.-Y. Ng *et al.*, Int. J. Mod. Phys. A (Proc. Suppl.) **2B**, 1049 (1993).
[18] I. Kourbanis, J. MacLachlan, and K. Meisner, Fermilab Report No. **EXP-172**, 1991 (unpublished).
[19] K. Y. Ng, Fermilab Internal Report No. TM-1389, 1986 (unpublished).
[20] J. Crisp, Fermilab Internal Report No. EXP-139, 1987 (unpublished).
[21] M. K. Craddock *et al.*, IEEE Trans. Nucl. Sci. **NS-24**, (3) 1615 (1977).
[22] S. Adam *et al.*, IEEE Trans. Nucl. Sci. **NS-28** (3) 2721 (1981).
[23] I. Kourbanis, K. Meisner, and K. Ng, Fermilab Report No. **TM-1696**, 1990 (unpublished), p. 141.
[24] J. Dey *et al.*, *IEEE Proceedings of the Particle Accelerator Conference, Washington, D.C.* (IEEE, New York, 1993), p. 1223.
[25] C. M. Bhat, *IEEE Proceedings of the Particle Accelerator Conference, Washington, D.C.* (IEEE, New York, 1993), p. 787.
[26] R. G. Scala and K. Meisner, *IEEE Proceedings of the Particle Accelerator Conference, Washington, D.C.* (IEEE, New York, 1993), p. 2519.
[27] M. A. Martens, *IEEE Proceedings of the Particle Accelerator Conference, Washington, D.C.* (IEEE, New York, 1993), p. 1963.
[28] L. M. Earley *et al.*, IEEE Trans. Nucl. Sci. **NS-30** (4), 3511 (1983).
[29] P. E. Faugeras *et al.*, in *IEEE Proceedings of the Particle Accelerator Conference, Washington, D.C.*, edited by E. R. Lindstorm and L. S. Taylor (IEEE, New York, 1987), p. 1719.
[30] T. Ieiri and G. Jackson, Fermilab Report No. **TM-1600**, 1989 (unpublished).